ACS Catalysis

Research Article

Cite This: ACS Catal. 2018, 8, 3965−3970

pubs.acs.org/acscatalysis

Engineering Ultrathin C_3N_4 Quantum Dots on Graphene as a Metal-Free Water Reduction Electrocatalyst

Hai-xia Zhong,[†,∥] Qi Zhang,[†,§,∥] Jun Wang,[†] Xin-bo Zhang,[‡] Xiao-lin Wei,[§] Zhi-jian Wu,[‡] Kai Li,[‡] Fan-lu Meng,[†] Di Bao,[‡] and Jun-min Yan*[,†]

[†]Key Laboratory of Automobile Materials (Jilin University), Ministry of Education, Department of Materials Science and Engineering, Jilin University, Changchun 130022, People's Republic of China

[‡]State Key Laboratory of Rare Earth Resource Utilization, Changchun Institute of Applied Chemistry, Chinese Academy of Sciences, Changchun 130022, People's Republic of China

[§]Hunan Key Laboratory for Micro-Nano Energy Materials and Device, Xiangtan University, Hunan 411105, People's Republic of China

Supporting Information

ABSTRACT: Developing an efficient electrocatalyst with the desired architectural and electronic properties is paramount for water splitting. Here, we apply theoretical calculations to experimental studies to uncover the influence of structure engineering (quantizing and support coupling) on the HER catalytic activity and develop an optimized C_3N_4 hybrid catalyst. Impressively, the desired atom-thick C_3N_4 quantum dots on graphene (CNQDs@G) has been successfully obtained and achieves HER performance with low overpotential (110 mV) at 10 mA cm^{-2}, large exchange current density (3.67 μA cm^{-2}), and long-term durability, better than those of many metallic catalysts. In combination with the experimental results, DFT calculations also disclose that the HER catalytic activity of CNQDs@G originates from bisynergetic effects: one between G and CNQDs and another between the edge pyridinic-N sites and the molecular sieve structure.

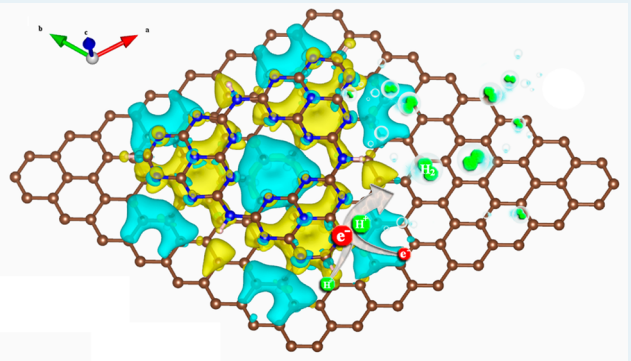

KEYWORDS: *quantum dots, atom-thick, bisynergistic effects, hydrogen evolution, theoretical predictions*

INTRODUCTION

Electrochemical water splitting into hydrogen, coupled with renewable energy (wind and solar energy), has become paramount in implementing sustainable energy conversion and storage technologies.[1] As the cathodic step, the hydrogen evolution reaction (HER) is widely advocated as the key process, in which optimized electrocatalysts are imperative to accelerate the reaction kinetics.[2,3] Therein, crucial factors including definite active sites, electron/mass transport properties, stability, and accessible synthesis routes should be considered to develop an advanced electrocatalyst. To date, various effective HER electrocatalysts including the state of the art Pt based metallic catalysts have been achieved.[4−7] Nevertheless, the exploration of a low-cost catalyst with the desired active sites, a special electronic structure, and thus excellent catalytic activity is ongoing for practical applications.[8−11]

One class of promising alternatives is a carbon-based metal-free material, such as graphitic carbon nitride (g-C_3N_4).[8,12−14] g-C_3N_4, with rich hydrogen absorption sites, strong stability, and tunable structure, has been successfully applied in photocatalytic HER, while its electrocatalytic performance is restricted by its high electrical resistance.[15,16] Recently, composition and structure adjustments have been used to greatly enhance the HER performances of C_3N_4 hybrid catalysts.[17] Nevertheless, its inferior performance in comparison to Pt still makes its potential in electrocatalysis uncertain, which is probably due to deficient understanding of the correlation of the structure engineering and the electronic/chemical properties of C_3N_4 hybrid electrodes and the origin of HER catalytic activity.[18,19] Fortunately, theoretical calculations in combination with experimental studies provide a feasible access to these issues, guiding a rational reaction-oriented catalyst design.[19,20] For example, the Shao-Horn group revealed that a special electronic structure is important to control the metal oxide catalytic activity for the OER and ORR using theoretical and experimental means, stimulating an extensive development of various metal oxide electrocatalysts.[21,22] Therefore, integrating theoretical calculations with experimental methods to study the correlations of the structure engineering and the electronic/

Received: February 7, 2018
Revised: March 21, 2018
Published: March 28, 2018

DOI: 10.1021/acscatal.8b00467
ACS Catal. 2018, 8, 3965−3970

chemical properties is greatly important and extremely challenging in exploring a robust C_3N_4-based electrocatalyst.

Inspired by previous works,[16,23] downsizing C_3N_4 and supporting it on a conductive substrate can effectively increase its catalytic activity in terms of increased exposed active sites and sufficient electron transfer. Therefore, first, we apply DFT calculations to investigate the support import and structure quantization effects on the electronic/chemical properties of the C_3N_4 hybrids and thus predict that g-C_3N_4 quantum dots (CNQDs) supported on graphene (CNQDs@G) with a sufficient charge-transfer capacity and abundant accessible edge sites would result in excellent HER catalytic activity. Next, the controlled synthesis of ultrathin CNQDs@G with uniform and well-dispersed CNQDs on G is achieved via a facile strategy. Indeed, this CNQDs@G exhibits high HER performance with low overpotential (110 mV) at 10 mA cm^{-2}, even comparable to those of many metallic catalysts. In addition, DFT calculation results and the experimental observations indicate that this mainly stems from bisynergistic effects: one between the intramolecular edge sites and the molecular sieve structure of CNQDs and another between CNQDs and G, different from the case for other C_3N_4 hybrid electrocatalysts. Despite enriching the active sites, C_3N_4 quantization also induces the transfer of the active sites from the internal pyridine N to the edge pyridine N and thus causes a different catalytic mechanism. These results highlight the importance of quantization and support importing in tailoring the electronic properties, creating the desired active sites and thus improving the catalytic activity, benefiting future rational electrocatalyst design.

EXPERIMENTAL SECTION

Chemicals and Materials. H_2SO_4 (≥95%, Sigma-Aldrich), H_3PO_4 (85%, Sigma-Aldrich), graphite flakes (flakes, 99% carbon basis, 325 mesh particle size, Sigma-Aldrich), $KMnO_4$ (97%, Sigma-Aldrich), H_2O_2 (30 wt % in H_2O, Sigma-Aldrich), and Melamine (99%, Sigma-Aldrich) were obtained from the sources indicated.

Preparation of Atom-Thick CNQDs@G. Atom-thick CNQDs@G was prepared by coupling the GO and CNQDs at a weight ratio of 5/1. CNQDs were added to the GO solution (10 mg mL^{-1}) with stirring, and then the mixture was transferred to an autoclave and heated at 150 °C for 1 h. Finally, atom-thick CNQDs@G was obtained by the heat treatment of CNQDs@GO at 400 °C for 2 h under an Ar atmosphere at 5 °C min^{-1}.

Characterization. The morphology of as-prepared samples was investigated by scanning electron microscopy (SEM, field emission Hitachi S-4800 instrument) and transmission electron microscopy (TEM, a FEI Tecnai G2 S-Twin instrument). Atomic force microscopy (AFM) was performed with a Bruker Dimension Icon apparatus. The as-prepared samples were also characterized by powder X-ray diffraction (XRD) measurements (a Bruker D8 Focus powder X-ray diffractometer using Cu Kα (λ = 0.15405 nm) radiation) and Fourier transform infrared (FT-IR) spectra (a Nicolet 6700 spectrometer). X-ray photoelectron spectroscopy (XPS) measurements were performed on an ESCALAB 250 photoelectron spectrometer. The electrochemical experiments were carried out with a VMP3 electrochemical workstation (Biologic VMP3).

Electrochemical Tests. All of the electrochemical measurements were performed on a rotating disk electrode (RDE, PINE, 5 mm) at a scan rate of 10 mV/s in 0.5 M H_2SO_4. A graphite rod (TianJin AIDA heng sheng Science-Technology Development Co., Ltd.) and a saturated calomel electrode (SCE) acted as the counter electrode and reference electrode, respectively. Typically, 10 mg of catalyst was dispersed by sonication in 1 mL of ethanol containing 100 μL of Nafion solution. Then the catalyst ink (10 μL) was drop-cast onto the glassy-carbon (GC) electrode with a catalyst loading of 0.485 mg cm^{-2}. The solution was purged with Ar gas for 60 min prior to the start of electrolysis under standard atmospheric pressure. During the chronoamperometric measurement, the generated gas was monitored with a gas buret, wherein carbon paper loaded with the catalyst was the working electrode. The impedance was tested by electrochemical impedance spectroscopy (EIS) measurements with an ac voltage of 10 mV amplitude in the frequency range from 100 kHz to 0.1 Hz at −0.4 V vs RHE. All of the polarization curves were corrected with 85% *iR* compensation with the built-in program, and all of the potentials were calibrated to a reversible hydrogen electrode (RHE).

Faradaic efficiency (FE) can be analyzed by the equation

$$\mathrm{FE} = (V/V_m \times 2/3)/(Q/F \times 1/2) \quad (1)$$

where Q is the quantity of electric charge (C), F is the Faraday constant (96485 C mol^{-1}), V (L) is the volume of the detected gas, and V_m is the molar volume (22.4 L mol^{-1}).

RESULTS AND DISCUSSION

Theoretical Predictions for the HER Activities of CNQDs@G. First-principles calculations were conducted to investigate the electronic structure of the materials and optimize the catalyst design.[8,24,25] First, graphene was chosen as the conductive support for its high electronic conductivity but negligible HER performance.[8,26,27] As a density of states (DOS) analysis (Figure 1a,b and Figure S1) revealed, g-C_3N_4 nanosheets on graphene (CNNSs@G) and CNQDs@G have good metallicity in comparison to the support-free counterparts.[28] Bader charge calculations further confirm their greatly improved electron mobility (Figure 1e). Meanwhile, downsizing g-C_3N_4 from CNNSs to CNQDs was used to increase the exposed active sties. Unexpectedly, quantization of C_3N_4 causes the redistribution of the charge density in the interlayer and the transfer of charge density difference mainly at the edges of CNQDs in the hybrids, which may act as active sites, greatly increasing the amount of active sites (Figure 1c,d and Figures S2−S4). Moreover, quantization also induces more charge transfer and enhanced electron coupling effects between the active component and graphene (Figure 1e). The higher adsorption energy (Figure 1e and Figure S2) further confirms the stronger interaction between CNQDs and G, benefiting the superior charge transfer kinetics during the HER process.

Generally, the HER occurs via proton adsorption and reduction on the catalyst surface to form H*, followed by H_2 formation and desorption processes.[29] Accordingly, the Gibbs free energy of the intermediate state (ΔG_{H^*}), as the crucial descriptor in the theoretical prediction of HER activity (the best value is 0 eV), is calculated to estimate the potential of CNQDs@G.[19,29] Figure 1f and Figures S5 and S6 reveal that CNQDs@G possesses smaller $|\Delta G_{H^*}|$ (0.1 eV) in comparison to CNNSs, CNNSs@G, G and CNQDs, and this value is even close to that of the state of the art Pt catalyst ($|\Delta G^{Pt}_{H^*}|$ = 0.09 eV). Thus, CNQDs@G with superior charge transfer capacity and abundant edge active sites should be an excellent HER electrocatalyst.

DOI: 10.1021/acscatal.8b00467
ACS Catal. 2018, 8, 3965−3970

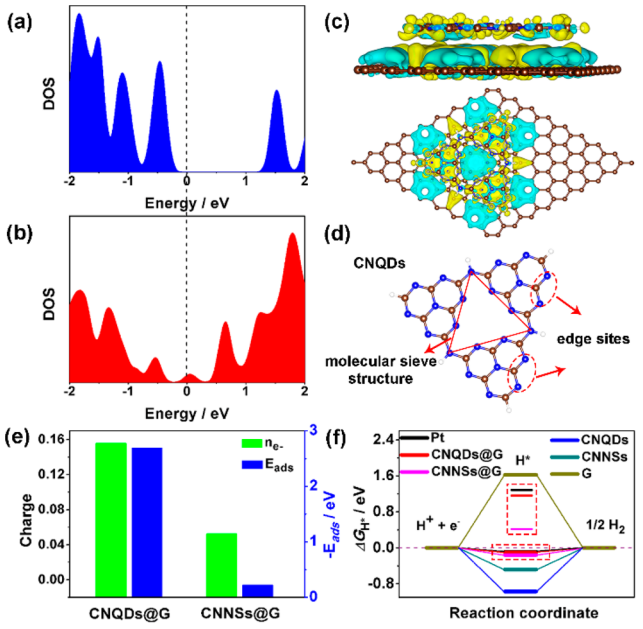

Figure 1. (a, b) Density of states for CNQDs and CNQDs@G. (c) Interfacial electron transfer in CNQDs@G (yellow and cyan isosurfaces represent electron accumulation and electron depletion, respectively, the isosurface value is 0.001 e Å^{-3}). (d) Schematic structure of CNQDs. (e) Bader charge analysis (n_{e-}: charge transfer) and adsorption energy (E_{ads}) of CNNSs@G and CNQDs@G. (f) Free energy diagrams for hydrogen evolution at the equilibrium potentials of G, CNNSs, CNQDSs, CNNSs@G, CNQDs@G and Pt reference.

Atom-Thick CNQDs@G with the Corresponding Characterizations. Accordingly, the CNQDs@G hybrid was synthesized (Figure 2a). First, CNQDs were obtained via a liquid exfoliation of bulk g-C_3N_4, verified by the absence of the typical g-C_3N_4 diffraction for CNQDs and the quantum effect

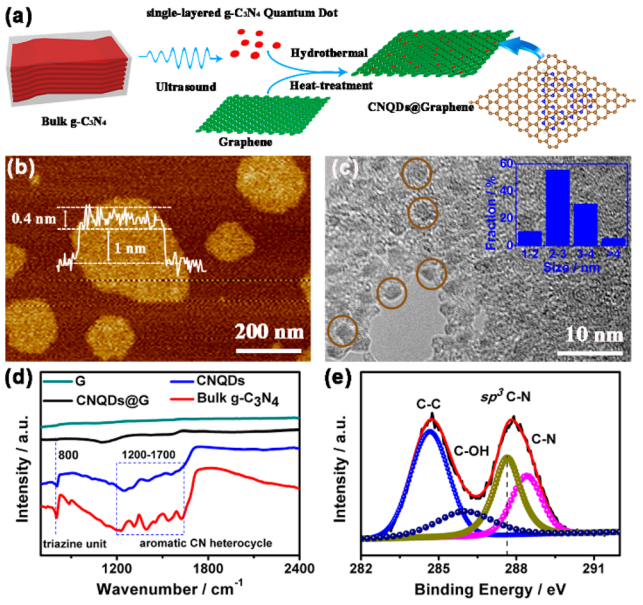

Figure 2. (a) Schematic synthesis process of CNQDs@G hybrid. (b) AFM image of CNQDs@G (inset: the corresponding height curve). (c) TEM image of CNQDs@G (inset: the corresponding size distribution). (d) FT-IR spectra of bulk g-C_3N_4, CNQDs, G, and CNQDs@G. (e) High-resolution C 1s XPS spectra of CNQDs@G.

features (Figures S8 and S9).[30] In addition, the characteristic peaks of FT-IR spectra for CNQDs are observed at 800 and 1200−1700 cm^{-1}, which belong to the deformation of tri-*s*-triazine ring modes and typical C−N heterocyclic stretches (Figure 2d and Figure S7),[31,32] respectively, further confirming the successful synthesis of CNQDs. Transmission electron microscopy (TEM) and atomic force microscopy (AFM) images (Figure S10) reveal the uniform size (3 nm) and atomic thickness (0.4 nm), which is favorable for further hybridization with graphene. After a hydrothermal hybridization with graphene oxide and a subsequent heating reduction process, CNQDs@G is obtained, as identified by XRD patterns and FT-IR and UV−visible absorption spectra (Figures S8 and S9c and Figure 2). AFM analysis shows that the thickness of CNQDs@G (1.4 nm) approaches the sum of that for CNQDs (0.4 nm) and G (1 nm), suggesting the intimate contact of CNQDs and G (Figure 2b and Figures S10b and S11b). The TEM image of CNQDs@G shows that uniform CNQDs without any obvious changes are evenly distributed on the graphene surface (Figure 2c), exposing more active sites and accelerating electron transfer. Additionally, it is worth noting that controlling the synthesis conditions (hydrothermal temperature, time, and ratio of CNQDs and graphene oxide) is important for fabricating uniformly dispersed CNQDs on graphene without any aggregation and morphology changes (details in Figures S12−S14 in the Supporting Information).

To further probe the chemical structure of CNQDs@G, X-ray photoelectron spectroscopy (XPS) was performed (Figure 2e and Figure S15). The high-resolution C 1s XPS spectrum shows that the peak for the in-plane C−C coordination of G is shifted to 284.8 eV due to the decoration of CNQDs on the G surface.[23] Moreover, the observation of a peak for the specific out-of-plane sp^3 C−N species at 287.2 eV verifies the interfacial interaction of CNQDs and G, which will result in an electron coupling effect between them and promote the electron transfer. The high-resolution N 1s XPS can be deconvoluted into three main peaks: C−N═C (398.6 eV), N−$(C)_3$ (399.7 eV), and C−NH (400.7 eV).[31] Therefore, these experimental observations imply that a well-designed CNQDs@G based on the theoretical calculations is successfully obtained.

Electrocatalytic HER Activity Evaluation. The HER electrocatalytic activity of CNQDs@G was evaluated in an acidic electrolyte. For a good comparison, the electrochemical performances of CNQDs, G, the physical mixture of CNQDs and G (CNQDs+G), CNNSs@G, and the commercial Pt/C were also investigated. In comparison to the extremely negative onset potential for CNQDs, CNQDs+G shows a more positive onset potential and increased current density due to the improved conductivity (Figure 3a and Table S1), indicating the important role of the conductive support in improving the catalytic performance of C_3N_4 materials. Remarkably, CNQDs@G has enhanced electron conductivity and much smaller overpotential (110 mV) at 10 mA cm^{-2} in comparison to CNQDs+G, very close to that for Pt/C (Figure S16 and Table S1), suggesting the synergistic HER catalytic activity of CNQDs and G in the hybrid. Therefore, G not only acts as the conductive support but also synergistically catalyzes the HER. Consistent with the prediction, CNNSs@G shows inferior HER catalytic activity with larger overpotential in comparison to CNQDs@G due to fewer easily accessible active sites. Furthermore, electrochemical impedance spectroscopy (EIS, Figure 3b) measurement was carried out to gain insight into the electron transfer kinetics. Lower charge-transfer resistance is

DOI: 10.1021/acscatal.8b00467
ACS Catal. 2018, 8, 3965−3970

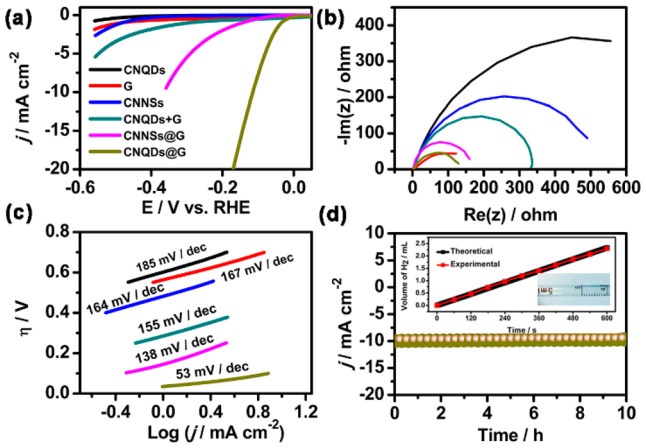

Figure 3. HER polarization curves at a scan rate of 10 mV s^{-1} (a), EIS (b), and Tafel plots (c) for CNNSs, CNQDs, G, CNQDs+G, CNNSs@G, and CNQDs@G in 0.5 M H_2SO_4. (d) Chronoamperometric responses of CNQDs@G at −0.11 V vs RHE (inset: the corresponding theoretical and experimental amounts of H_2).

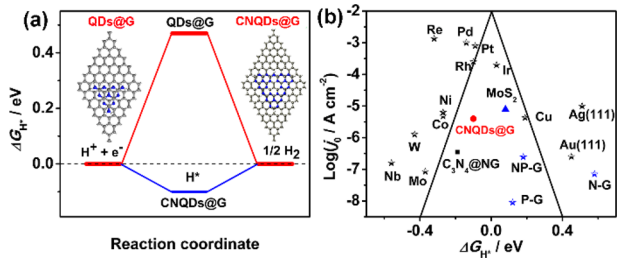

Figure 4. (a) Free energy diagrams for hydrogen evolution at the equilibrium potential of CNQDs@G and QDs@G (inset: their schematic structure). (b) Volcano plot of j_0 as a function of ΔG_{H^*} for CNQDs@G and other catalysts.

observed for CNQDs@G during the HER process in comparison to the counterpart samples, demonstrating its faster electron-transfer kinetics.[31] which is the prime requirement for an efficient electrocatalyst. Furthermore, the superior HER catalytic activity of CNQDs@G is also gleaned from its smaller Tafel slope (53 mV dec^{-1}, Figure 3c), in comparison to the control samples (CNQDs, G, CNQDs+G, and CNNSs@G), implying more favorable reaction kinetics[33] and a possible Volmer−Heyrovsky reaction pathway with the electrochemical desorption of hydrogen as the rate-limiting step at the CNQDs@G electrode.[23] Accordingly, the calculated exchange current density (j_0) of CNQDs@G is 3.67 uA cm^{-2}, which is even comparable to those for many metallic catalysts, further highlighting its superiority for the HER (Table S2).[34] Thus, coupling with a conductive support and quantizing C_3N_4 can effectively improve the HER catalytic activity of C_3N_4 hybrids.

Stability of CNQDs@G. As another paramount factor for practical applications, the stability of CNQDs@G has been assessed by chronoamperometric techniques. As shown in Figure 3d, CNQDs@G exhibits a negligible current density loss after 10 h continuous electrolysis with no obvious morphology and structure changes (Figure S17), which is associated with the intrinsic stability and strong interaction of CNQDs and G. However, Pt/C suffers an apparent current reduction under identical conditions, suggesting the superior stability of CNQDs@G. In addition, the agreement of the theoretical and experimental amounts of hydrogen suggests that the Faradaic efficiency at CNQDs@G electrode is almost 100% (the inset image in Figure 3d), wherein little loss is due to the dissolved gas in the electrolyte and the attached bubbles at the electrode surface.

Bisynergistic Effects. The HER process on the catalyst surface has also been investigated. The ΔG_{H^*} value for C_3N_4 materials (CNQDs and CNNSs) or G is negative or positive, indicating the difficult adsorption or desorption behavior of H*, respectively.[19,23] Meanwhile, CNQDs@G has an appropriate ΔG_{H^*} value and thus faster reaction kinetics toward the HER, indicating the synergistic contribution of CNQDs and G to the better HER catalytic activity (Figure 1f). Therein, the edge pyridine N sites show smaller $|\Delta G_{H^*}|$ values in comparison to the in-plane pyridine N in the molecular sieve structure of CNQDs in the hybrids, further confirming the transfer of the active sites from the internal defects to the edge sites (Figure 1c and Figure S19). Next, idealized C_3N_4 QDs on graphene (QDs@G) with only edge sites were studied to identify the role of the in-plane molecular sieve structure (Figure 4a and Figures S20−S22). A larger $|\Delta G_{H^*}|$ value and lower HER catalytic activity is obtained for QDs@G in comparison to those for CNQDs@G, illustrating the synergistic catalysis of the molecular sieve structure and the edge sites at CNQDs@G electrodes. It is thus clear that the superior catalytic activity of CNQDs@G can be attributed to bisynergistic effects: one between G and CNQDs and another among the edge sites and the molecular sieve structure of CNQDs@G. Note that the according rate-limiting step of CNQDs@G varies with different applied potential, resulting in a different reaction mechanism at the CNQDs@G electrode (Figure S23). At a low overpotential, the rate-limiting step is electrochemical desorption of hydrogen (Volmer−Heyrovsky mechanism), while at a high overpotential the chemical desorption of hydrogen is the rate-limiting step (Volmer−Tafel mechanism). In addition, a volcano plot of j_0 as a function of the ΔG_{H^*} value has been applied to emphasize the superior catalytic activity of CNQDs@G, wherein the value of a better catalyst is much closer to the peak. Figure 4b shows that CNQDs@G is one of the best metal-free HER electrocatalysts, even superior to many metallic alternatives.[23,35−38]

CONCLUSIONS

In conclusion, theoretical calculations and experimental results both verify that rational structure engineering (graphene coupling and quantizing C_3N_4) will result in an improved charge transfer capacity and increased density of active sites and thus superior HER catalytic activity for C_3N_4 hybrids. Expectedly, the obtained atom-thick CNQDs@G has a high HER performance that is comparable to that of many metallic electrocatalysts. More importantly, combining the theoretical and experimental means, we also have determined that its superior performance arises from bisynergistic effects (G and CNQDs; the edge sites and the typical molecular sieve structure of CNQDs). These findings identify the importance of structure adjustment in designing highly active, durable, and cost-effective HER electrocatalysts, which can be suitable for other related catalyst design. In addition, we also expect that the strategy of integrating theoretical and experimental means to explore an effective electrocatalyst can be expanded to develop electrocatalysts for other energy-related fields.

DOI: 10.1021/acscatal.8b00467
ACS Catal. 2018, 8, 3965−3970

■ ASSOCIATED CONTENT

Supporting Information

The Supporting Information is available free of charge on the ACS Publications website at DOI: 10.1021/acscatal.8b00467.

Calculation details (methods and models), the synthesis process, and various characterization data (XRD, XPS, FT-IR, TEM, SEM) (PDF)

■ AUTHOR INFORMATION

Corresponding Author

*E-mail for J.Y.: junminyan@jlu.edu.cn.

ORCID

Xin-bo Zhang: 0000-0002-5806-159X

Jun-min Yan: 0000-0001-8511-3810

Author Contributions

‖H.Z. and Q.Z. contributed equally to this work.

Notes

The authors declare no competing financial interest.

■ ACKNOWLEDGMENTS

This work was supported in part by the National Natural Science Foundation of China (51522101, 51472209, 51471075, and 51631004) and the program for the JLU Science and Technology Innovative Research Team (2017TD-09).

■ REFERENCES

(1) Karunadasa, H. I.; Chang, C. J.; Long, J. R. A molecular molybdenum-oxo catalyst for generating hydrogen from water. *Nature* **2010**, *464*, 1329−1333.

(2) Jiao, Y.; Zheng, Y.; Davey, K.; Qiao, S. Z. Activity origin and catalyst design principles for electrocatalytic hydrogen evolution on heteroatom-doped graphene. *Nat. Energy* **2016**, *1*, 16130.

(3) Norskov, J. K.; Christensen, C. H. Toward efficient hydrogen production at surfaces. *Science* **2006**, *312*, 1322−1323.

(4) Fan, Z.; Luo, Z.; Huang, X.; Li, B.; Chen, Y.; Wang, J.; Hu, Y.; Zhang, H. Synthesis of 4H/fcc noble multimetallic nanoribbons for electrocatalytic hydrogen evolution reaction. *J. Am. Chem. Soc.* **2016**, *138*, 1414−1419.

(5) Lv, H.; Xi, Z.; Chen, Z.; Guo, S.; Yu, Y.; Zhu, W.; Li, Q.; Zhang, X.; Pan, M.; Lu, G. A new core/shell NiAu/Au nanoparticle catalyst with Pt-like activity for hydrogen evolution reaction. *J. Am. Chem. Soc.* **2015**, *137*, 5859−5862.

(6) Morales-Guio, C. G.; Stern, L. A.; Hu, X. Nanostructured hydrotreating catalysts for electrochemical hydrogen evolution. *Chem. Soc. Rev.* **2014**, *43*, 6555−6569.

(7) Yin, J.; Fan, Q.; Li, Y.; Cheng, F.; Zhou, P.; Xi, P.; Sun, S. Ni-C-N nanosheets as catalyst for hydrogen evolution reaction. *J. Am. Chem. Soc.* **2016**, *138*, 14546−14549.

(8) Deng, D.; Novoselov, K. S.; Fu, Q.; Zheng, N.; Tian, Z.; Bao, X. Catalysis with two-dimensional materials and their heterostructures. *Nat. Nanotechnol.* **2016**, *11*, 218−230.

(9) Shi, Y.; Zhang, B. Recent advances in transition metal phosphide nanomaterials: synthesis and applications in hydrogen evolution reaction. *Chem. Soc. Rev.* **2016**, *45*, 1529−1541.

(10) Zheng, Y.; Jiao, Y.; Zhu, Y.; Cai, Q.; Vasileff, A.; Li, L. H.; Han, Y.; Chen, Y.; Qiao, S. Z. Molecule-level g-C_3N_4 coordinated transition metals as a new class of electrocatalysts for oxygen electrode reactions. *J. Am. Chem. Soc.* **2017**, *139*, 3336−3339.

(11) Zou, X.; Zhang, Y. Noble metal-free hydrogen evolution catalysts for water splitting. *Chem. Soc. Rev.* **2015**, *44*, 5148−5180.

(12) Liang, J.; Zheng, Y.; Chen, J.; Liu, J.; Hulicova-Jurcakova, D.; Jaroniec, M.; Qiao, S. Z. Facile oxygen reduction on a three-dimensionally ordered macroporous graphitic C_3N_4/carbon composite electrocatalyst. *Angew. Chem., Int. Ed.* **2012**, *51*, 3892−3896.

(13) Ma, T. Y.; Dai, S.; Jaroniec, M.; Qiao, S. Z. Graphitic carbon nitride nanosheet-carbon nanotube three-dimensional porous composites as high-performance oxygen evolution electrocatalysts. *Angew. Chem., Int. Ed.* **2014**, *53*, 7281−7285.

(14) Zhang, X.; Xie, X.; Wang, H.; Zhang, J.; Pan, B.; Xie, Y. Enhanced photoresponsive ultrathin graphitic-phase C_3N_4 nanosheets for bioimaging. *J. Am. Chem. Soc.* **2013**, *135*, 18−21.

(15) Wang, X.; Maeda, K.; Thomas, A.; Takanabe, K.; Xin, G.; Carlsson, J. M.; Domen, K.; Antonietti, M. A metal-free polymeric photocatalyst for hydrogen production from water under visible light. *Nat. Mater.* **2009**, *8*, 76−80.

(16) Zhao, Y.; Zhao, F.; Wang, X.; Xu, C.; Zhang, Z.; Shi, G.; Qu, L. Graphitic carbon nitride nanoribbons: graphene-assisted formation and synergic function for highly efficient hydrogen evolution. *Angew. Chem., Int. Ed.* **2014**, *53*, 13934−13939.

(17) Duan, J. J.; Shen, C.; Jaroniec, M.; Qiao, S. Z. Porous C_3N_4 nanolayers@ N-graphene films as catalyst electrodes for highly efficient hydrogen evolution. *ACS Nano* **2015**, *9*, 931−940.

(18) Jiao, Y.; Zheng, Y.; Jaroniec, M.; Qiao, S. Z. Origin of the electrocatalytic oxygen reduction activity of graphene-based catalysts: a roadmap to achieve the best performance. *J. Am. Chem. Soc.* **2014**, *136*, 4394−4403.

(19) Seh, Z. W.; Kibsgaard, J.; Dickens, C. F.; Chorkendorff, I.; Norskov, J. K.; Jaramillo, T. F. Combining theory and experiment in electrocatalysis: insights into materials design. *Science* **2017**, *355*, eaad4998.

(20) Wang, J.; Li, K.; Zhong, H. X.; Xu, D.; Wang, Z. L.; Jiang, Z.; Wu, Z. J.; Zhang, X. B. C and N hybrid coordination derived Co-C-N complex as a highly efficient electrocatalyst for hydrogen evolution reaction. *J. Am. Chem. Soc.* **2015**, *137*, 15070−15073.

(21) Suntivich, J.; Gasteiger, H. A.; Yabuuchi, N.; Nakanishi, H.; Goodenough, J. B.; Shao-Horn, Y. Design principles for oxygen-reduction activity on perovskite oxide catalysts for fuel cells and metal-air batteries. *Nat. Chem.* **2011**, *3*, 546−550.

(22) Suntivich, J.; May, K. J.; Gasteiger, H. A.; Goodenough, J. B.; Shao-Horn, Y. A perovskite oxide optimized for oxygen evolution catalysis from molecular orbital principles. *Science* **2011**, *334*, 1383−1385.

(23) Zheng, Y.; Jiao, Y.; Zhu, Y.; Li, L. H.; Han, Y.; Chen, Y.; Du, A.; Jaroniec, M.; Qiao, S. Z. Hydrogen evolution by a metal-free electrocatalyst. *Nat. Commun.* **2014**, *5*, 3783.

(24) Skulason, E.; Tripkovic, V.; Bjorketun, M. E.; Gudmundsdottir, S.; Karlberg, G.; Rossmeisl, J.; Bligaard, T.; Jonsson, H.; Norskov, J. K. Modeling the electrochemical hydrogen oxidation and evolution reactions on the basis of density functional theory calculations. *J. Phys. Chem. C* **2010**, *114*, 18182−18197.

(25) Gao, G.; Jiao, Y.; Ma, F.; Jiao, Y.; Waclawik, E.; Du, A. Metal-free graphitic carbon nitride as mechano-catalyst for hydrogen evolution reaction. *J. Catal.* **2015**, *332*, 149−155.

(26) Du, A. In silico engineering of graphene-based van der Waals heterostructured nanohybrids for electronics and energy applications. *WIREs. Comput. Mol. Sci.* **2016**, *6*, 551−570.

(27) Ito, Y.; Cong, W.; Fujita, T.; Tang, Z.; Chen, M. High catalytic activity of nitrogen and sulfur co-doped nanoporous graphene in the hydrogen evolution reaction. *Angew. Chem., Int. Ed.* **2015**, *54*, 2131−2136.

(28) Ghosh, D.; Periyasamy, G.; Pati, S. K. Transition metal embedded two-dimensional C_3N_4−graphene nanocomposite: a multifunctional material. *J. Phys. Chem. C* **2014**, *118*, 15487−15494.

(29) Norskov, J. K.; Bligaard, T.; Rossmeisl, J.; Christensen, C. H. Towards the computational design of solid catalysts. *Nat. Chem.* **2009**, *1*, 37−46.

(30) Zhang, X.; Wang, H.; Wang, H.; Zhang, Q.; Xie, J.; Tian, Y.; Wang, J.; Xie, Y. Single-layered graphitic-C_3N_4 quantum dots for two-photon fluorescence imaging of cellular nucleus. *Adv. Mater.* **2014**, *26*, 4438−4443.

(31) Wang, J.; Li, K.; Zhong, H. X.; Xu, D.; Wang, Z. L.; Jiang, Z.; Wu, Z. J.; Zhang, X. B. Synergistic effect between metal-nitrogen-carbon sheets and NiO nanoparticles for enhanced electrochemical

DOI: 10.1021/acscatal.8b00467
ACS Catal. 2018, 8, 3965−3970

water-oxidation performance. *Angew. Chem., Int. Ed.* **2015**, *54*, 10530−10534.
(32) Du, X.; Zou, G.; Wang, Z.; Wang, X. A scalable chemical route to soluble acidified graphitic carbon nitride: an ideal precursor for isolated ultrathin g-C_3N_4 nanosheets. *Nanoscale* **2015**, *7*, 8701−8706.
(33) Liu, Y.; Cheng, H.; Lyu, M.; Fan, S.; Liu, Q.; Zhang, W.; Zhi, Y.; Wang, C.; Xiao, C.; Wei, S. Low overpotential in vacancy-rich ultrathin CoSe2 nanosheets for water oxidation. *J. Am. Chem. Soc.* **2014**, *136*, 15670−15675.
(34) Kita, H. Periodic variation of exchange current density of hydrogen electrode reaction with atomic number and reaction mechanism. *J. Electrochem. Soc.* **1966**, *113*, 1095−1111.
(35) Jaramillo, T. F.; Jørgensen, K. P.; Bonde, J.; Nielsen, J. H.; Horch, S.; Chorkendorff, I. Identification of active edge sites for electrochemical H_2 evolution from MoS_2 nanocatalysts. *Science* **2007**, *317*, 100.
(36) Nørskov, J. K.; Bligaard, T.; Logadottir, A.; Kitchin, J. R.; Chen, J. G.; Pandelov, S.; Stimming, U. Trends in the exchange current for hydrogen evolution. *J. Electrochem. Soc.* **2005**, *152*, J23.
(37) Peng, Y.; Pan, W. Z.; Wang, N.; Lu, J. E.; Chen, S. W. Ruthenium ion-complexed graphitic carbon nitride nanosheets supported on reduced graphene oxide as high-performance catalysts for electrochemical hydrogen evolution. *ChemSusChem* **2018**, *11*, 130.
(38) Peng, Y.; Lu, B. Z.; Chen, L. M.; Wang, N.; Lu, J. E.; Ping, Y.; Chen, S. W. Hydrogen evolution reaction catalyzed by ruthenium ion-complexed graphitic carbon nitride nanosheets. *J. Mater. Chem. A* **2017**, *5*, 18261−18269.

DOI: 10.1021/acscatal.8b00467
ACS Catal. 2018, 8, 3965−3970